*Full Length Research Paper*

# A simplified mathematical model of multi-species biofilm for simultaneous removal of sulfur dioxide (SO$_2$) and nitric oxide (NO) using a biotrickling-filter

**Yaqiong Han, Weijiang Zhang\* and Jiao Xu**

School of Chemical Engineering and Technology, Tianjin University, Tianjin 300072, China.

The population dynamics of a multi-species biofilm for simultaneous removal of nitric oxide (NO) and sulfur dioxide (SO$_2$) in a laboratory-scale biotrickling-filter was described. Based on a simplified multispecies-multisubstrate model with the gas-liquid-biomembrane transfer theory, the calculations were compared to the long-term verification experiments. Simulation results were in good agreement with the experimental values of biofilm thickness, population densities of biofilm, total biomass dry weight and partial pressures of NO and SO$_2$ in the outlet gas. The model has been proven to be capable of describing the dynamic biofilm growth, multiple biomass evolution and synergetic effect between sulfate reducing bacteria and denitrifying bacteria on simultaneous removal of NO and SO$_2$. When NO feed concentration was constant at 1780 mg/m$^3$ and SO$_2$ feed concentration was shifted between 0 and 3200 mg/m$^3$ every half hour, the removal efficiencies of NO and SO$_2$ at steady-state were above 90 and 95%, both in the simulation and experiment.

**Key words:** Population dynamics, multispecies-multisubstrate, gas-liquid-biomembrane transfer, biotrickling-filter, simultaneous SO$_2$ and NO removal.

**INTRODUCTION**

Acid precipitation is a current air pollution problem caused mainly by SO$_2$ and NOx (±95% NO and ±5% NO$_2$) (Maas et al., 2008). Over the years, various approaches have been developed for combined removal of SO$_2$ and NO from flue gas, including chemical radiation (Chmielewski et al., 2000), pulsed-corona discharges (Mok and Nam, 2002), selective catalytic reduction (Tronconi et al., 2005), adsorption (Wilde et al., 2001) and microbiology methods (Dasu et al., 1993). As a result of low-temperature, low-consumption, low-cost, simplicity of operation and no secondary pollution, microbial treat-ment of waste gas is considered as a promising alternative technique. In order to better understand this microbial technology, further work should be performed to invest-igate the biodegradation dynamics and the process simulation.

Several models have been proposed for simulation of biodegradation dynamics and kinetics for waste gas treatment. The model proposed by Hodge and Devinny (1995) assumed a unified and combined biofilm-solid phase where the biodegradation reactions take place following first order kinetics. However, the details of the pollutant behavior in the biofilm were ignored in this model (Jorio et al., 2003). In the improved models, biofilms were considered as the multiple-phase systems where a liquid phase fills the pores and cavities of a sponge-type structure of a solid phase (Picioreanu et al., 2004a; Hekmat et al., 2006), moreover, the under-standing of biofilms structure has been developed to regard the biofilms as the multispecies communities (Stoodley et al., 2002). However, this multispecies biofilms represent quite complex dynamic systems, and due to this complexity, current understanding of biofilm systems for waste gas treatment is limited (Hekmat et al., 2006). Only little work exists on the description of modeling of the multispecies biofilm population dynamics for waste gas removal, but all these models are concerned with the

―――――――――
\*Corresponding author. E-mail: zzw@tju.edu.cn. Tel: +86-13642014092. Fax: +86-22-58299574.

treatment of volatile organic compounds (VOC's) (Hekmat et al., 2006; Champagne et al., 1999; Den and Pirbazari, 2002). Therefore, there has been an increasingly urgent need to establish a simplified multispecies- multisubstrate model for simultaneous removal of $SO_2$ and NO.

In order to investigate the multispecies biofilm population dynamics as well as its kinetic relationships for simultaneous removal of $SO_2$ and NO, the present study aimed at developing a simplified model and compared the modeling results with the verification experiment data. Meanwhile, we firstly proposed the gas-liquid-biomembrane transfer theory (an extended two-film theory), which is used to simulate the gas transfer process from the bulk gas phase to cell membrane through the liquid phase. This combination of hydromechanics performance and biofilm growth dynamics helps to obtain a more realistic and reasonable simulation.

## MATERIALS AND METHODS

### Model description

The biotrickling-filter used for simultaneous bioremoval of NO and $SO_2$ contains three compartments: gas, liquid and biofilm. The biofilm grows on the surface of a packing material. And it is assumed that the transport of all substrates consisting of $SO_2$ ($S_1$), NO ($S_2$) and $H_2S$ ($S_3$) takes place only by molecular diffusion.

This multi-species biofilm mainly consists of sulfate reducing bacteria ($X_A$) and denitrifying bacteria ($X_B$), in which the interaction is that of $H_2S$, the end product of $SO_2$ reduction by sulfate reducing bacteria ($SO_2 \to H_2S$), which serves as the primary electron donor for the reduction of NO by denitrifying bacteria ($H_2S + NO \to SO_4^{2-} + N_2$). Sulfate reducing bacteria (SRB) and denitrifying bacteria (DB) are subjected to detachment and inactivation. The latter process leads to an inactive population ($X_P$).

Generally, structure of a mature biofilm can be depicted as polymer matrix with open spongiform structure, which is typically below 0.2 mm thick and contain 75 to 90% water of its wet weight (Helle et al., 2000). For simplification, the density of solid phase in the biofilms is assumed to be constant and there is no active biomass suspended in the liquid phase and no attachment of biomass takes place. With the dry biomass concentrations of cells $X_i$ (i = A, SRB; B, DB; P, inactive cells), the liquid porosity $\varepsilon_l$ and the constant cell dry biomass densities $\rho_i$, we got the biofilm composition equation:

$$X_i / \rho_i + \varepsilon_l = 1$$
$$i = A, B \text{ and } P \tag{1}$$

### Mass balance of the active biomass

Substrate-limiting Monod kinetics is applied to describe the specific growth rate of the cell populations in the biofilm. Moreover, the cell inactivation rate is formulated as being linearly proportional to the cell concentration and the detachment rate is proportional not only to the cell concentration but to the square of the biofilm thickness

$L_f$ (Picioreanu et al., 2004a). Thus, the growth rates of the species A and B are given by:

$$\frac{dX_i}{dt} = growth\ rate - inactivation\ rate + detachment\ rate, i = A, B$$

$$\frac{dX_A}{dt} = \mu_{max,A1} X_A \frac{S_1}{K_{A1} + S_1} - b_A X_A - \lambda L_f^2 X_A \sigma_w \tag{2}$$

$$\frac{dX_B}{dt} = \mu_{max,B2} X_B \frac{S_2}{K_{B2} + S_2} - b_B X_B - \lambda L_f^2 X_B \sigma_w \tag{3}$$

### Mass balance of the inactive biomass

The growth rate of inactive biomass is given by:

$$\frac{dX_P}{dt} = inactivation\ rate + detachment\ rate$$

$$\frac{dX_P}{dt} = b_A X_A + b_B X_B - \lambda L_f^2 X_P \sigma_w \tag{4}$$

### Mass balance of the solutes in the biofilm

The diffusion-reaction rates of solutes (dissolved substrates of $SO_2$, NO and $H_2S$) in the biofilm are given by:

$$\frac{dS_1}{dt} = \sigma_w J_1 + \frac{k_{31}}{k_{23}} \frac{\omega_{23}}{\omega_{23}} \frac{\mu_{max,B2}}{Y_{B2}} X_B \frac{S_2}{K_{B2}+S_2} \frac{S_3}{K_{B3}+S_3} - \frac{\mu_{max,A1}}{Y_{A1}} X_A \frac{S_1}{K_{A1}+S_1} \tag{5}$$

$$\frac{dS_2}{dt} = \sigma_w J_2 - \frac{\mu_{max,B2}}{Y_{B2}} X_B \frac{S_2}{K_{B2} + S_2} \frac{S_3}{K_{B3} + S_3} \tag{6}$$

$$\frac{dS_3}{dt} = \frac{k_{13}}{\omega_{13}} \frac{\mu_{max,A1}}{Y_{A1}} X_A \frac{S_1}{K_{A1}+S_1} - \frac{k_{23}}{\omega_{23}} \frac{\mu_{max,B2}}{Y_{B2}} X_B \frac{S_2}{K_{B2}+S_2} \frac{S_3}{K_{B3}+S_3} \tag{7}$$

$J_1$ and $J_2$ of Equations (5) and (6) are the overall mass transfer fluxes of $SO_2$ and NO which are transferred from the gas phase into the biofilm through the liquid phase, respectively.

### The growth rate of the biofilm thickness

Growth of cells results in an increase of the biofilm thickness, so the growth rate of biofilm thickness can be easily obtained as follows:

$$\frac{dL_f}{dt} = \frac{L_f}{1-\varepsilon_l} \times (\frac{dX_A}{\rho_A dt} + \frac{dX_B}{\rho_B dt} + \frac{dX_P}{\rho_P dt}) \tag{8}$$
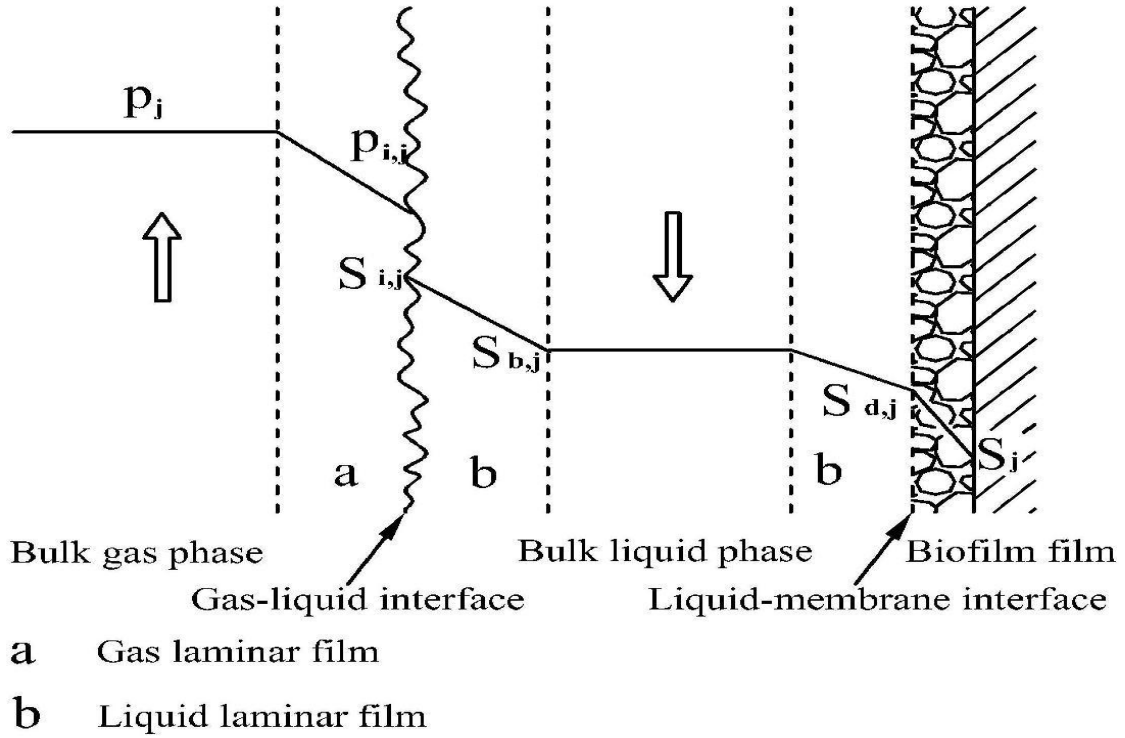
**Figure 1.** Schematic description of gas-liquid-biomembrane mass transfer mechanism.

### Gas-liquid-biomembrane mass transfer

The process of the gas-liquid-biomembrane mass transfer is illustrated in Figure 1. The steady-state mass transfer can be assumed within an infinitesimal time step, so the diffusion flux $\upsilon_{g,j}$ (j = 1 for $SO_2$ and j = 2 for NO) through the gas laminar film to the gas-liquid interface, must be equal to the diffusion flux $\upsilon_{l,j}$ through the liquid laminar film to the bulk liquid, and equal to the diffusion flux $\upsilon_{d,j}$ through the laminar diffusional sub layer surrounding the biofilm to the surface of biofilm, and equal to diffusion flux $\upsilon_{m,j}$ through the cell membrane

$$J_j = \upsilon_{g,j} = \upsilon_{l,j} = \upsilon_{d,j} = \upsilon_{m,j}$$ (9)

$$\upsilon_{g,j} = \frac{k_{g,j}(S^*_j - S_{i,j})}{H_j}$$ (10)

$$\upsilon_{l,j} = k_{l,j}(S_{i,j} - S_{b,j})$$ (11)

$$\upsilon_{d,j} = \frac{D_{l,j}(S_{b,j} - S_{d,j})}{L_l}$$ (12)

$$\upsilon_{m,j} = D_{m,j}\frac{(S_{d,j} - S_j)}{L_m}$$ (13)

According to Henry's Law, $S^*_j$ is the concentration in equilibrium with its corresponding partial pressure in the bulk gas, and Henry's constants $H_j$ can be derived from Henry's coefficient; $S_{i,j}$ is the gas-liquid interfacial concentration; $S_{b,j}$ is the concentration in the bulk liquid; $S_{d,j}$ is the concentration in the liquid laminar film surrounding the biofilm and $S_j$ is the concentration in the biofilm. Adding Equations (10) to (13) to Equation (9), we get the overall mass transfer coefficient:

$$K_{L,j} = 1 \left/ \left( \frac{H_j}{k_{g,j}} + k_{l,j} + \frac{L_l}{D_{l,j}} + \frac{L_m}{\upsilon_{m,j}} \right) \right.$$ (14)

So the overall mass transfer flux can be written in $K_{L,j}$ form:

$$J_j = K_{L,j}(S^*_j - S_j)$$ (15)

### $SO_2$ and NO outlet partial pressures

The $SO_2$ and NO concentrations in the bulk gas phase are the

**Table 1.** Initial values and fitted model parameters of the model.

| Parameters | Value |
|---|---|
| Initial solute concentration of dissolved SO$_2$, NO and H$_2$S in the biofilm, $S_j(0), j=1,2,3$ (g/m$^3$) | 0 |
| Initial biofilm thickness, $L_f(0)$ (m) | 6×10$^{-5}$ |
| Maximum specific growth rate of SRB on SO$_2$, $\mu_{\max,A1}$ (h$^{-1}$) | 0.124 |
| Maximum specific growth rate of DB on NO, $\mu_{\max,B2}$ (h$^{-1}$) | 0.99 |
| Saturation constant of SRB on SO$_2$, $K_{A1}$ (g/m$^3$) | 8 |
| Saturation constant of DB on NO, $K_{B2}$ (g/m$^3$) | 0.022 |
| Saturation constant of DB on H$_2$S, $K_{B3}$ (g/m$^3$) | 2 |
| Yield of SRB on SO$_2$, $Y_{A1}$ | 0.12 |
| Yield of DB on NO, $Y_{B2}$ | 0.44 |
| Stoichiometric ratio of SO$_2$ to H$_2$S by SRB, $\omega_{13}$ | 1 |
| Stoichiometric ratio of NO to H$_2$S by DB, $\omega_{23}$ | 4 |
| Decay rate constant of SRB, $b_A$ (h$^{-1}$) | 0.003 |
| Decay rate constant of DB, $b_B$ (h$^{-1}$) | 0.005 |
| Decay rate constant of inactive biomass, $b_P$ (h$^{-1}$) | 0.005 |
| Biomass detachment velocity constant, $\lambda$ (m$^{-1}$h$^{-1}$) | 116.7 |

height-time functions. Thus, the SO$_2$ and NO gas concentrations at any time can be obtained from a simple mass balance along the filter height, that is, SO$_2$ and NO being removed from the gas phase is equal to the amount entering into the biofilm (Liu et al., 1998). The outlet gas partial pressure at the top of filter at any time $P_{top,j}$ ($P_{top,j} = S^*_{top,j}/H_j M_j$) is derived from the differential equation for counter flow operation:

$$-\frac{\partial S^*_j(Z,t)}{\partial Z} = K_{L,j}(S^{..}_j(Z,t) - S_j(t))\times\frac{\sigma_w}{\upsilon_g} \tag{16}$$

Where $S^*_j$ (same as in Equation (10)) is the concentration in equilibrium with its corresponding partial pressure in the bulk gas and $M_j$ is the substrate mole mass. With the boundary conditions: $S^{..}_j(Z=0) = S_{btm,j}$ and $S^{..}_j(Z=H_t) = S_{top,J}$, we got SO$_2$ and NO outlet partial pressures:

$$P_{top,j}(t) = \frac{S^*_{top,j}(t)}{H_i M_i} = \frac{(S_{btm,j}(t) - S_j(t))\exp(-K_{L,j}\sigma_w\tau) + S_j(t)}{H_i M_i} \tag{17}$$

where $\tau = H_t/\upsilon_g$ is the average gas residence time.

### Model parameters

The model parameters in Table 1 (except initial parameters) were obtained from a fit to the experimental data using the common method of least squares. The parameters in Table 2 were obtained from the relevant literature. Based on the conditions earlier mentioned, the model was programmed with Matlab 7.0.

### Biotrickling filter setup and operation

A schematic of the experimental setup is shown in Figure 2. To validate the proposed biofilm model, a 160 day verification experiment was performed in a biotrickling-filter. The bioreactor geometry and the operating conditions are given in Table 3. The filter was filled with the polyethylene Cascade Rings (25 × 13 × 1 mm; specific surface area of 228 m$^2$/m$^3$; porosity of 90% m$^3$/m$^3$; bulk density of 65 kg/m$^3$; filling rate of 75%). Additionally, the filter was operated at a constant temperature (30 ± 0.5°C) with the heating tape which was controlled by a digital temperature controller (AI-708P, China). The pH of the recirculation liquid was controlled at 7.0 ± 0.1 via a pH controller (Knick model 761, Germany) that automatically added 5 wt% NaHCO$_3$ solutions to the liquid.

The landfill leachate used as the seed inoculum was obtained from a municipal landfill in Tianjin, China. After being inoculated, the filter was operated continuously for gas and liquid in a counter-current operation. To keep the dynamic balance between the supply and demand of H$_2$S, the feed concentration of SO$_2$ was shifted between 0 and 3200 mg/m$^3$ every half hour according to the model results, while that of NO was maintained constant at 1780 mg/m$^3$. SO$_2$, NO and N$_2$ contained in the feed gas were supplied from compressed gas cylinders and then mixed in the gas mixer before entering the filter. The fluxes of SO$_2$, NO and N$_2$ were controlled by the gas flow meters. More detailed operating processes can be seen

**Table 2.** Model parameters were obtained from the previous literature or book.

| Parameters | Value |
| --- | --- |
| Mass transfer boundary layer thickness, $L_l$ (m) | $7.2 \times 10^{-5}$ [*] |
| Density of active biomass, $\rho_A$, $\rho_B$ (g/m$^3$) | $2 \times 10^{5}$ [*] |
| Density of inactive biomass, $\rho_p$ (g/m$^3$) | $3.3 \times 10^{4}$ [*] |
| Volume fraction of liquid in biofilm, $\varepsilon_l$ | $0.8$ [*] |
| Diffusion coefficient of SO$_2$ through the cell membrane, $D_{m1}$ (m$^2$/s) | $6.35 \times 10^{-12}$ [†] |
| Diffusion coefficient of NO through the cell membrane, $D_{m2}$ (m$^2$/s) | $8.48 \times 10^{-12}$ [§] |
| cell membrane thickness, $L_m$ (m) | $8 \times 10^{-9}$ [§] |
| Diffusion coefficient of SO$_2$ in liquid, $D_{l1}$ (m$^2$/s) | $1.46 \times 10^{-9}$ [¶] |
| Diffusion coefficient of NO in liquid, $D_{l2}$ (m$^2$/s) | $2.2 \times 10^{-9}$ [¶] |
| SO$_2$ gas phase mass transfer coefficient, $k_{g1}$ (m/s) | $8.18 \times 10^{-8}$ [¶] |
| NO gas phase mass transfer coefficient, $k_{g2}$ (m/s) | $2.77 \times 10^{-7}$ [¶] |
| SO$_2$ liquid phase mass transfer coefficient, $k_{l1}$ ( mol·m$^{-2}$·pa$^{-1}$·s$^{-1}$) | $7.38 \times 10^{-4}$ [¶] |
| NO liquid phase mass transfer coefficient, $k_{l2}$ (mol·m$^{-2}$·pa$^{-1}$·s$^{-1}$) | $9.05 \times 10^{-4}$ [¶] |
| Henry coefficient of SO$_2$, $E_1$ (kPa 30 ) | $0.485 \times 10^{4}$ [¶] |
| Henry coefficient of NO, $E_2$ (kPa 30 ) | $3.14 \times 10^{6}$ [¶] |
| Mole mass ratio of H$_2$S to SO$_2$, $k_{31}$ | 0.53 |
| Mole mass ratio of H$_2$S to NO, $k_{32}$ | 1.13 |

[*]Alpkvist et al. (2006); [†]Kuehne and Frledlander (1980); [§]Chen et al. (1998); [¶]McCabe et al. (1993).

in the previous literature (Ingvorsen et al., 2003; Philip and Deshusses, 2003).

### Analyses

The concentrations of NO, SO$_2$ and H$_2$S in the inlet and outlet were determined by a flue gas analyzer (KANE940 Multi- Gas Emissions Analyser, UK). The concentrations of nitrate, nitrite, sulfate, sulfite, sulfide and the amount of protein were all determined by a water quality analyzer (Merck NOVA 60 Spectroquant, Germany). The number of SRB cells per carrier was measured using the fluorescence *in situ* hybridization (FISH) method with a probe (SRB385, China). The number of DB cells per carrier was measured by combined use of stable-isotope probing (SIP), full-cycle rRNA analysis, and FISH (Ginige et al., 2005). The thickness of biofilm was measured by the weight of the total amount of biomass on the surface of a single packing material using a biofilm density of 1 g/cm$^3$ and the total surface area of the packing material (1.45 cm$^2$). The total biomass dry weight per carrier was also measured using the gravimetrical method (Staudt et al., 2004).

## RESULTS AND DISCUSSION

The biofilm model was evaluated for the development of biofilm thickness, population density of the biofilm, total biomass dry weight per carrier and NO and SO$_2$ partial pressures in the outlet gas.

### Development of biofilm thickness

The biofilm thickness profile and the corresponding simulation result are shown in Figure 3. The model simulation basically agreed with the measurements of the biofilm thickness profile, indicating that the proposed model is able to simulate the growth of mixed-species biofilm for simultaneous bioremoval of NO and SO$_2$. The biofilm thickness initially increased with biofilm age and then became stable after 1000 h when the biofilm reached a steady-state from the adaptive phase.

### Multiple biomass evolution

As shown in Figure 4A and B, a good agreement was achieved between the simulated and measured results of the cell population densities and the total biomass dry weight per carrier. The simulation curves in Figure 4A showed that SRB gained the competition advantage at the first 2.5 h, because the fast-growing bacteria of SRB would take advantage of high SO$_2$ concentration, while the growth of denitrifying bacteria was limited by the supply of H$_2$S. In the next 4 h, the slow-growing bacteria of denitrifying bacteria obtained the relative higher rate due to the strong affinity for NO ( $K_{B2}$ is relatively smaller)
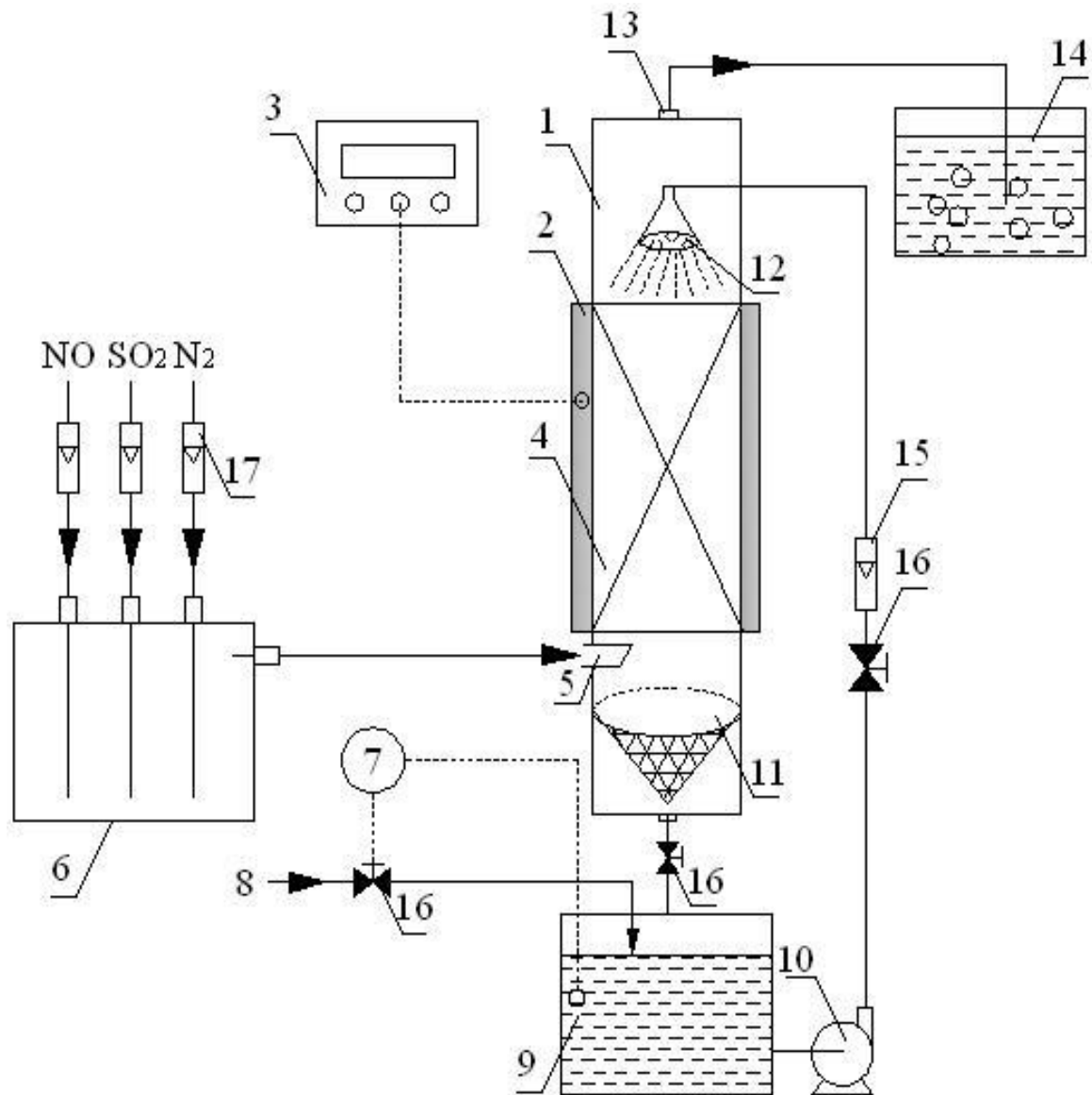
**Figure 2.** Schematic diagram of experimental setup. 1, Combined removal NOx/SO₂ biotrickling filter; 2, heating tape; 3, temperature controller; 4, packings; 5, gas inlet; 6, gas mixer; 7, pH controller; 8, NaHCO₃ solution; 9, recycle liquid reservoir; 10, pump; 11, preventing clogging net; 12, liquid distributor; 13, gas outlet; 14, gas absorber; 15, liquid flow meter; 16, valve; 17, gas flow meter.

**Table 3.** Bioreactor geometry and operating conditions in the experiments.

| Parameters | Value |
|---|---|
| Height of the biotrickling-filter, $H_t$ (m) | 2 |
| Inner diameter of biotrickling-filter, $D$ (m) | 0.08 |
| Gas flow rate, $\upsilon_g$ (m/s) | $3.4 \times 10^{-2}$ |
| Recirculating liquid flow rate, $\upsilon_l$ (m/s) | $6.6 \times 10^{-3}$ |
| Average gas residence time, $\tau$ (min) | 1 |
| SO₂ concentration in equilibrium with SO₂ partial pressure in the inlet gas, $S^*_{btm,1}$ (g/m³) | 120 |
| NO concentration in equilibrium with NO partial pressure in the inlet gas, $S^*_{btm,2}$ (g/m³) | 0.09 |
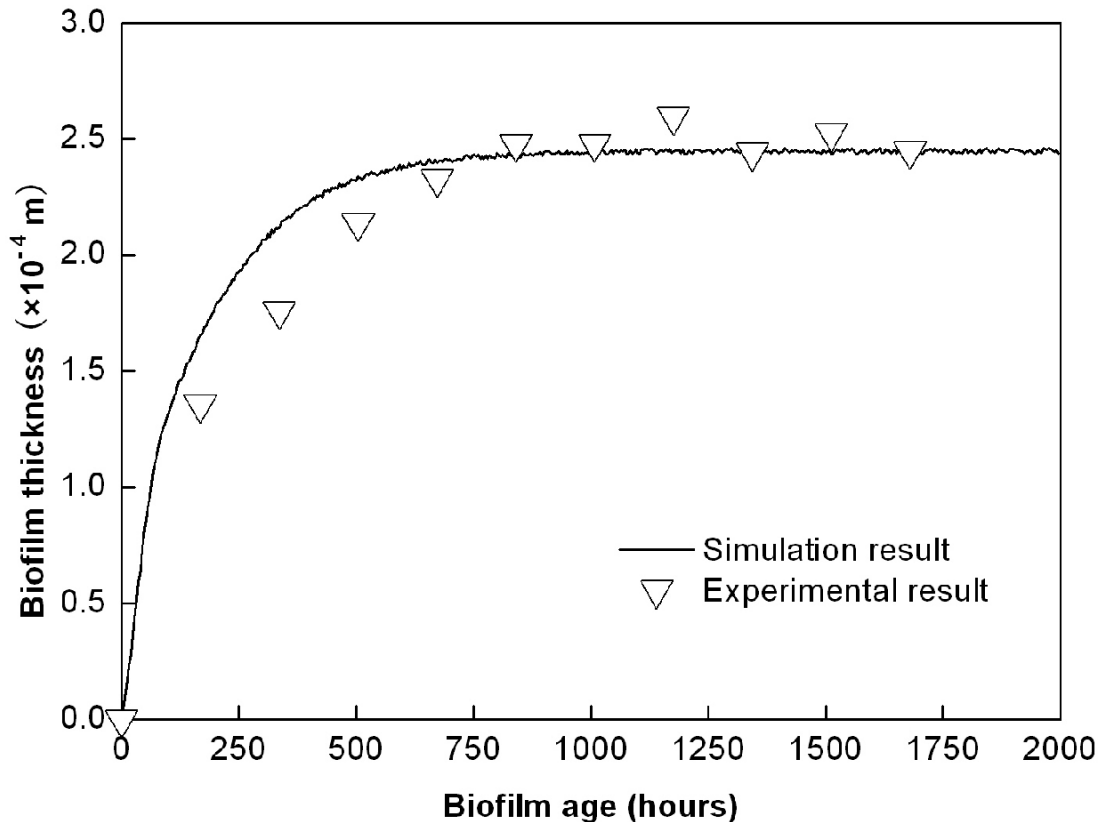
**Figure 3.** Comparison of simulated and measured development of the thickness of biofilm.

and the stable electron donor ($H_2S$) supply. Denitrifying bacteria maintained this competitive advantage with a higher population density until the 75th hour. And then, SRB eventually became dominant because: (1) SRB develop a symbiotic relationship with DB for establishment of a sulfur cycle to sustain higher energy requirements;
(2) heterotrophic bacteria such as SRB can produce the slime-like materials that help in adhering biofilms to the packing surfaces (Chou and Lin, 2000), so SRB have a better resistance to the hydrodynamic shear stress and finally achieve the competitive advantage.

The sufficiently thick biofilm was obtained after about 1000 h when transfer distances were long enough and substrates transport to inner bacteria cells became slow in comparison with the bioconversion kinetics of the microorganisms (Picioreanu et al., 2004b), so dynamic equilibrium between biomass growth and detachment was obtained and different biomass concentrations turned to be constant (Figure 4B).

**Performance of multi-species biofilm for simultaneous removal of NO and $SO_2$**

According to the simulation results, $SO_2$ feed concentration should be shifted between 0 and its peak

load every half hour to avoid the accumulation of $H_2S$, which is consistent with the experimental result that $H_2S$ outlet concentration with $SO_2$-shift feedings was always below 150 mg/m$^3$ (not shown). As shown in Figure 5, a satisfactory agreement between the model predictions and measured values of partial pressures in the outlet gas was achieved, although the latter was slightly greater than the model results with a higher fluctuation frequency, especially the NO outlet pressure. One of the reasons for this is that mass transfer can not be the ideal steady-state molecular diffusion (as assumed in 1.1 and 1.1.5) and always accompanied by the mass loss and convection, therefore, there is always fluctuations and deviations around the model results.

It is further shown by simulation that in the first 40 days, the NO outlet partial pressure abruptly dropped to 15 Pa from about 60 Pa with the removal efficiency of NO dramatically increasing to 91.7 from 66.7%. Then, the NO outlet partial pressure at steady-state was fluctuated with a narrow range around the value of 15 Pa over the next 120 days. By contrast, the $SO_2$ outlet partial pressure was always kept below 10 Pa throughout the entire process with the relatively higher removal efficiency above 95%. Both simulated and measured results showed that the NO removal efficiency was always lower than the $SO_2$ removal efficiency because of the relative insolubility of
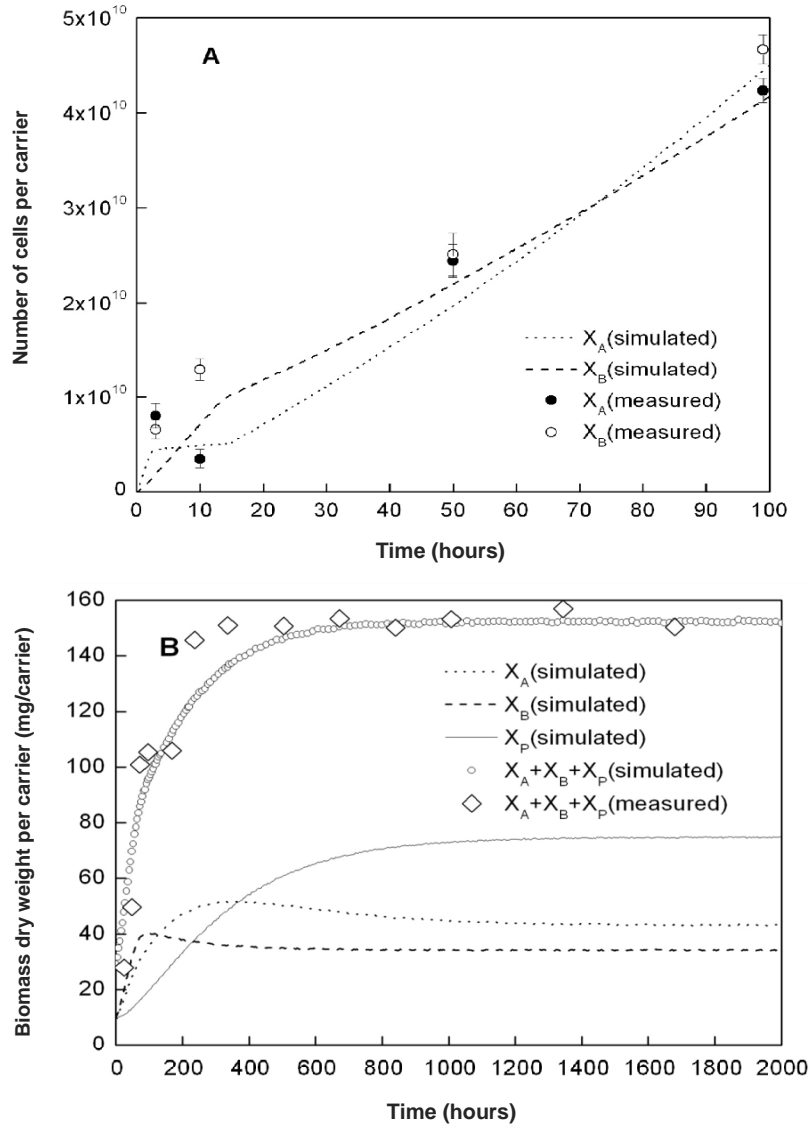
**Figure 4.** Time course of population densities of $X_A$, $X_B$ and $X_P$. (A) Comparison of the simulated and measured development of numbers of $X_A$, $X_B$ and $X_P$ per carrier; (B) development of the biomass dry weight of $X_A$, $X_B$ and $X_P$ per carrier in simulation and the total biomass dry weight per carrier both in simulation and experiment. $X_A$: SRB; $X_B$: DB; $X_P$: inactive cells

NO. More specifically, the assimilation of NO by bacteria is limited by the amount of NO into the biofilm, because the concentration difference to drive NO through the liquid laminar film to the biofilm is relatively small due to the low solubility of NO in liquid. Therefore, to increase the diffusion flux of NO into the biofilm, is crucial to further promote the NO biodegradation efficiency.

## Conclusions

This study developed a comprehensive biofilm model to predict pollutant bioremoval process and biofilm growth in a biotrickling-filter. The main conclusions drawn from this study are as follows:

1. The model is able to describe the dynamic biofilm growth, the multiple biomass evolution and the synergetic effect of SRB and denitrifying bacteria on simultaneous removal of NO and $SO_2$ in a biotrickling-filter.

2. The model has been extensively verified using the different approaches and an excellent agreement between the model predictions and measurements was achieved, including the thickness of biofilm, population densities of different species, total biomass dry weight of cells and the partial pressures of NO and $SO_2$ in the outlet gas.
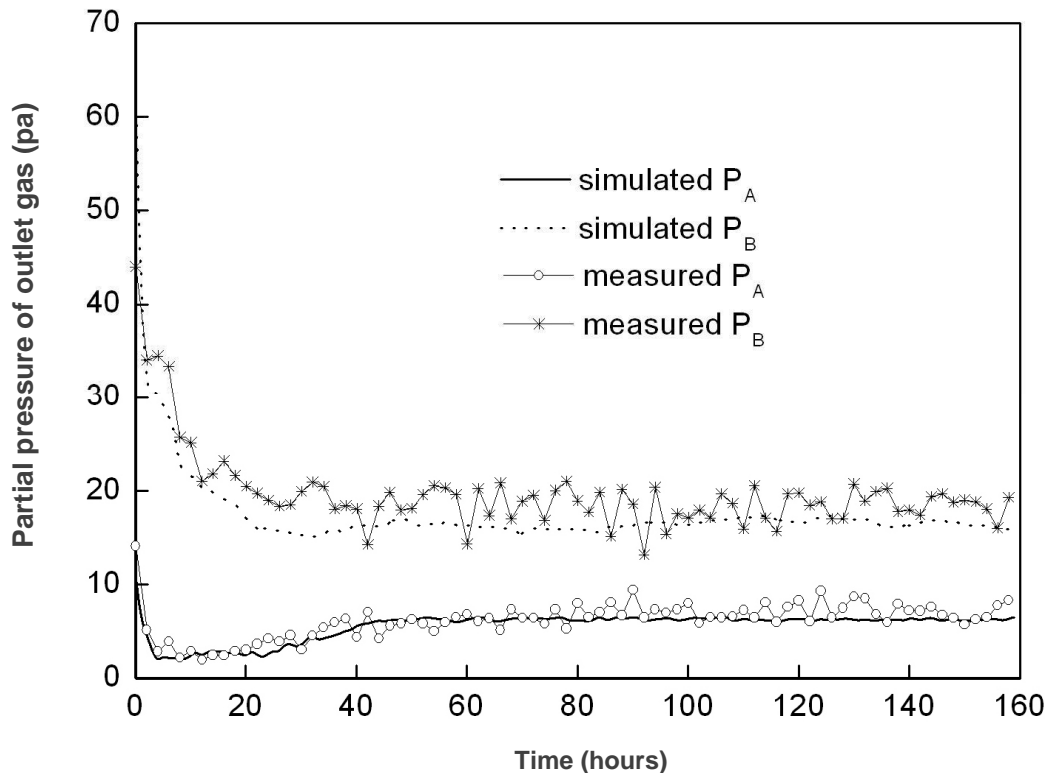
**Figure 5.** Comparison of simulated and measured development of the $SO_2$ outlet partial pressure ($P_A$) and NO outlet partial pressure ($P_B$). Either simulated or measured value is the average daily results.

3. Both in simulation and experiment, the removal efficiencies of NO and $SO_2$ at steady-state could be maintained above 90 and 95%, respectively.

## ACKNOWLEDGEMENT

## REFERENCES

Alpkvist E, Picioreanu C, Van Loosdrecht MCM, Heyden A (2006). Three-dimensional biofilm model with individual cells and continuum EPS matrix. Biotechnol. Bioeng., 94: 961-979.

Champagne P, Parker WJ, Van Geel P (1999). Modeling cometabolic biodegradation of organic compounds in biofilms. Water Sci. Technol., 39: 147-152.

Chen B, Keshive M, Deen WM (1998). Diffusion and reaction of nitric oxide in suspension cell cultures. Biophys. J., 75: 745-754.

Chmielewski AG, Tymiski B, Dobrowolski A, Iller E, Zimek Z, Licki J (2000). Empirical models for NOx and $SO_2$ removal in a double stage flue gas irradiation process. Radiat. Phys. Chem., 57: 527-530.

Chou MS, Lin JH (2000). Biotrickling filtration of nitric oxide. J. Air Waste Manage., 50: 502-508.

Dasu BN, Deshmane V, Shanmugasundram R, Lee CM, Sublette KL (1993). Microbial reduction of sulfur dioxide and nitric oxide. Fuel, 72: 1705-1714.

Den W, Pirbazari M (2002). Modeling and design of vapor-phase biofiltration for chlorinated volatile organic compounds. AIChE J., 48: 2084-2103.

Ginige MP, Keller J, Blackall LL (2005). Investigation of an acetate-fed denitrifying microbial community by stable isotope probing, full-cycle rRNA analysis, and fluorescent *in situ* hybridization-microautoradiography. Appl. Environ. Microb., 71: 8693-8691.

Hekmat D, Stephan M, Bauer R, Feuchtinger A, Vortmeyer D (2006). Modelling of multispecies biofilm population dynamics in a trickle-bed bioreactor used for waste gas treatment. Process. Biochem., 41: 1409-1416.

Helle H, Vuoriraznta P, Välimäki H, Lekkala J, Aaltonen V (2000). Monitoring of biofilm growth with thickness-shear mode quartz resonators in different flow and nutrition conditions. Sensor. Actuat. B-Chem., 71: 47-54.

Hodge DS, Devinny JS (1995). Modeling removal of air contaminants by biofiltration. J. Environ. Eng-Asce., 121: 21-32.

Ingvorsen K, Nielsen MY, Joulian C (2003). Kinetics of bacterial sulfate reduction in an activated sludge plant. FEMS Microbiol. Ecol., 46: 129-137.

Jorio H, Payre G, Heitz M (2003). Mathematical modeling of gas-phase biofilter performance. J. Chem. Technol. Biot., 78: 834-846.

Kuehne DL, Frledlander SK (1980). Selective transport of sulfur dioxide through polymer membranes. 1. polyacrylate and cellulose triacetate single-layer membranes. Ind. Eng. Chem. Process Des. Dev., 19: 609-616.

Liu XP, Miller MJS, Joshi MS, Sadowska-Krowicka H, Clark DA, Lancaster JR (1998). Diffusion-limited reaction of free nitric oxide with *Erythrocytes*. J. Biol. Chem., 273: 18709-18713.

Maas Pvd, Sandt Tvd, Klapwijk B, Lens P (2008). Biological reduction of nitric oxide in aqueous Fe(II)EDTA solutions. Biotechnol. Progr., 19: 1323-1328.

McCabe WL, Smith JC, Harriott P (1993). Unit operation of chemical engineering. 5th ed. Principles of diffusion and mass transfer

between phases, McGraw-Hill International Editions, New York, pp. 658-665.

Mok YS, Nam IS (2002). Modeling of pulsed corona discharge process for the removal of nitric oxide and sulfur dioxide. Chem. Eng. J., 85: 87-97.

Philip L, Deshusses MA (2003). Sulfur dioxide treatment from flue gases using a biotrickling filter-bioreactor system. Environ. Sci. Technol., 37: 1978-1982.

Picioreanu C, Kreft JU, Van Loosdrecht MCM (2004a). Particle-based multidimensional multispecies biofilm model. Appl. Environ. Microbiol., 70: 3024-3040.

Picioreanu C, Xavier JB, van Loosdrecht MCM (2004b). Advances in mathematical modeling of biofilm structure. Biofilms., 1: 337-349.

Staudt C, Horn H, Hempel DC, Neu TR (2004). Volumetric measurements of bacterial cells and extracellular polymeric substance glycoconjugates in biofilms. Biotechnol. Bioeng., 88: 585-592.

Stoodley P, Sauer K, Davies DG, Costerton JW (2002). Biofilms as complex differentiated communities. Ann. Rev. Microbiol., 56: 187-209.

Tronconi E, Beretta A, Elmi AS, Forzatti P, Malloggi S, Baldacci A (2005). A complete model of scr monolith reactors for the analysis of interacting NOx reduction and $SO_2$ oxidation reactions. Chem. Eng. Sci., 49: 4277-4287.

Wilde JD, Das AK, Heynderickx GH, Marin GB (2001). Development of a transient kinetic model for the simultaneous adsorption of SO2−NOx over Na/ -$Al_2O_3$ sorbent. Ind. Eng. Chem. Res., 40: 119-130.